

Microcracks in the alveolar bone following orthodontic tooth movement: a morphological and morphometric study

Carlalberta Verna*, Michel Dalstra*, T. Clive Lee**, Paolo M. Cattaneo* and Birte Melsen*

*Department of Orthodontics, Royal Dental College, University of Aarhus, Denmark and **Department of Anatomy, Royal College of Surgeons in Ireland, Dublin, Ireland

SUMMARY Microcracks and microdamage have been associated with bone remodelling. The aim of this study was to investigate the role of microcracks as a trigger for alveolar bone remodelling after the application of an orthodontic load.

In 25 3-month-old male Danish land-race pigs, the lower right first molar was moved buccally with a force of 130 cN. The contralateral molar was not treated and was used as an internal control. After 1, 2, 4, 7 and 15 days of treatment, the regions containing the right and left molars were excised and *en bloc* stained in basic fuchsin. The presence of microcracks on the buccal and lingual sides of both treated and untreated teeth was detected and expressed as crack density (number/mm²).

The buccal treated side showed significantly more cracks than the buccal untreated side at day 1. This difference was significantly larger than that observed at days 2, 7 and 15. The same side showed significantly more microcracks than the lingual treated side at day 1, and this difference was larger compared with that observed at days 4 and 15.

The presence of more microcracks on the treated side than on the untreated side suggests a role for microcracks in the initiation of bone remodelling after orthodontic loading. The increased presence of microcracks on the side towards which the tooth was moved, and where bone resorption is usually observed, suggests that microcracks could represent the first damage induced by orthodontic force that has to be repaired by bone remodelling.

Finally, the strain levels in the alveolar bone during the orthodontic load transfer in the experiment were examined by finite element (FE) analysis. Although this showed that the strains were very low (10–100 μ strain), it should be noted that occlusal loading was not taken into account. In addition, high-resolution microtomography of the alveolar bone/periodontal ligament (PDL) interface revealed that the actual surface of the alveolar bone was very rough, predisposing it to high local stress/strain peaks.

Introduction

The mechanical load applied to the alveolar bone through orthodontic devices initiates a cascade of biological events that ultimately leads to orthodontic tooth movement. In the area towards which the tooth is being moved, bone resorption occurs in both a direct and an indirect way (Reitan, 1967). Several hypotheses have been put forward in order to describe the first event that might initiate bone resorption in the direction of the force (Epker and Frost, 1965; Bien, 1966; Zengo *et al.*, 1973; Heller and Nanda, 1979; Davidovitch *et al.*, 1980, 1988; Sandy *et al.*, 1993; Tuncay *et al.*, 1994; Reitan and Rygh, 1994; Weinbaum *et al.*, 1994; Marotti, 1996; Melsen, 2001).

Recent concepts connecting bone mechanics and bone biology not only relate bone remodelling to the adaptation of the internal structure to load, but also to the need to remove fatigue damage (Lee *et al.*, 2002). Microdamage in bone was first described by Frost (1960) and is the epiphenomenon of fatigue, creep, or other accumulative mechanical processes that

permanently alter the microstructure (Martin, 2003). Microdamage is increased by fatigue loading at physiological strains and is associated with the activation of remodelling and osteocyte apoptosis (Verborgt *et al.*, 2000; Noble, 2003). Remodelling activated by, and in close proximity to, microdamage is described by some authors as ‘targeted’ remodelling as opposed to ‘random’ remodelling that could serve other functions, such as calcium homeostasis (Burr, 2002; Parfitt, 2002). Martin (2003) described four types of microdamage: (1) microcracks, commonly found in cortical bone, which extend approximately 100 μ m and are frequently limited by osteonal cement lines; (2) diffuse damage, more commonly found in sectioned trabeculae, appears as patches of more intensely stained mineralized matrix that have apparently been disrupted by locally intense deformations; (3) when small cracks appear in trabeculae as localized networks they are described as cross-hatching cracks; (4) microfractures are described when trabecular structures are completely fractured.

The principal mechanisms of matrix failure, according to Boyce *et al.* (1998), are strongly dependent on local strain. In regions subjected to tensile strains, the bone has diffuse microdamage, whereas in compressive strain regions the tissue develops linear microcracks.

Jaw bones are subjected to cyclic load, as chewing is rhythmic in nature (Gerstner, 1998; Gerstner and Cianfarani, 1998). During a 24-hour observation period, most high-amplitude bursts of the masseter muscle appear mainly during mealtimes, whereas a substantially larger number of low-amplitude bursts of the masseter muscle are distributed throughout the whole day (Miyamoto *et al.*, 1999). It is thus hypothesized that bone in the jaws is subjected to fatigue loading and microdamage could occur. The application of an orthodontic load may represent a further mechanical perturbation that causes damage to accumulate in alveolar bone.

The aim of this study was to investigate the role of microcracks as a trigger for alveolar bone remodelling after the application of an orthodontic load.

Materials and methods

Animal study

In 25 3-month-old male Danish land-race pigs, the lower right first molar was moved buccally with a force of approximately 130 cN. The research protocol was approved by the Danish Board for Animal Research (Dyreforsøgstilsynet). The biomechanical set-up consisted of a statically determined system where the force was applied by means of a custom-made cantilever made of a TMA 0.017 × 0.025 inch wire (Figure 1). The contralateral molar was not treated and was used as an internal control, according to a split-mouth study design. The appliances were applied under general anaesthesia. Pre-medication was performed with an intramuscular injection of midazolam (1 ml/10 kg body weight) and azaperon (1 ml/10 kg body weight). Otracheal intubation was set up after an intravenous injection of etomidate [25 per cent of body weight (kg) in ml]. Anaesthesia was maintained by inhalation of a mixture of CO₂, O₂, NO₂ and isoflurane (1–2.5 per cent), supplemented by an intravenous administration of fentanyl (1–2.5 µg/kg). After fitting the appliance, the animals were housed in individual sties and fed a standard diet for pigs (Die Plus FI, Axelborg, Copenhagen, Denmark). The animals were divided into five groups, according to treatment duration: groups 1, 2, 3, 4 and 5 were treated for 1, 2, 4, 7 and 15 days, respectively. At the end of treatment, the animals were killed by an intracardiac injection of an overdose of pentobarbital.

At sacrifice, the entire mandible was excised and fixed in 75 per cent alcohol. From each mandible the

region of interest around the lower first molar was further excised, to a size of approximately 2.5 × 2 × 1 cm. The samples were *en bloc* stained in basic fuchsin to label microdamage (Lee *et al.*, 1998). This method has been used for compact bone and a few adjustments had to be made in order to take into consideration the presence of soft tissue, represented by the periodontal ligament (PDL). Therefore, the final staining protocol was as follows: 0.5 per cent basic fuchsin in 80 per cent ethanol (2 × 45 minutes); 0.5 per cent basic fuchsin in 90 per cent ethanol (2 × 45 minutes); 0.5 per cent basic fuchsin in 99 per cent ethanol (2 × 45 minutes); 99 per cent ethanol (1 hour); washed in distilled water (2 × 24 hours), and finally air dried. Consecutive coronal sections of 100 µm were cut parallel to the mesial root of the molar with an Exact-saw (Exact Medical Instruments Inc., Oklahoma City, Oklahoma, USA) using a cutting–grinding technique. The coronal halves of the alveolar bone surrounding the roots on the buccal and lingual sides of both the treated and untreated sides were analysed for each animal. For each tooth, two consecutive sections were analysed at ×20 magnification. To visualize microdamage, sections were analysed under transmitted light and both green ($\lambda = 546$ nm) and ultraviolet ($\lambda = 365$ nm) epifluorescence (Lee *et al.*, 1998). To define the minimum crack length, 15 osteocyte lacunae were randomly selected and the mean osteocyte lacunar length was measured (mean = 26.6 ± 4.1 µm). The minimum crack length was thus defined as being at least twice the length of an average osteocyte lacuna.

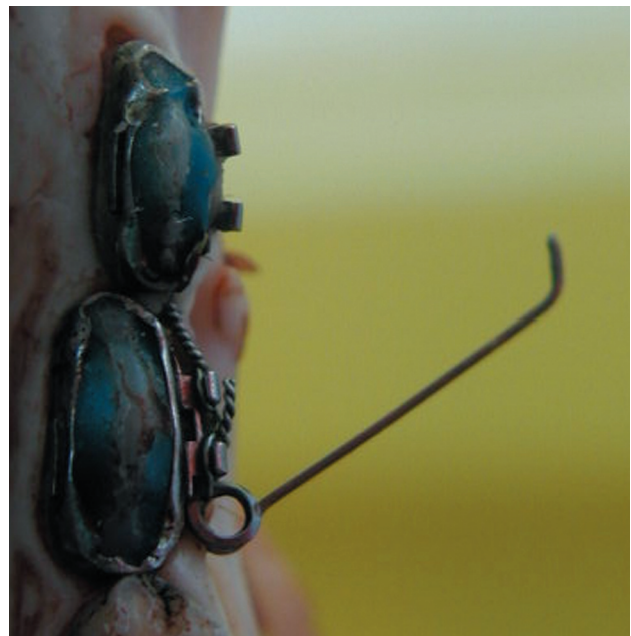


Figure 1 The orthodontic appliance consisted of a cantilever spring made of TMA 0.017 × 0.025 inch wire with single-point force application.

Measurements were performed on images captured on computer by a 3-CCD colour video camera (KY-F55B, JVC, Yokohama, Japan) mounted on the microscope and elaborated by dedicated software (Computer Assisted Stereology Toolbox, Olympus Danmark A/S, Ballerup, Denmark). The results were tabulated in the form of numerical crack density (number of cracks occurring per mm²). The error of the method, based on double measurements performed on 10 randomly selected sections by the same investigator (CV), was estimated according to Dahlberg's formula:

$$S = \sqrt{\sum d^2/2n}$$

where n is the number of paired measurements and d is the difference between the two measurements (Houston, 1983).

The data obtained for the buccal and lingual sides of the treated and untreated sides were compared within each animal, using paired data statistics. The data distribution was analysed by means of a Kolmerogov-Smirnoff test. When data were not normally distributed, non-parametric statistics were used. The Wilcoxon signed-ranks test was applied to perform paired comparisons between the buccal sides and between the lingual sides, and to compare the buccal and lingual sides of both the treated and untreated sides. In order to test both treatment effect and duration by keeping paired data, the differences between the treated and untreated sides and between the buccal and lingual sides were calculated and used as dependent variables. The effect of treatment duration was then tested by means of a Kruskal-Wallis test when data were not normally distributed or, in the case of normal distribution, by means of a one-way ANOVA. If a difference between groups was detected, and in order to identify which treatment time differed from another, a Mann-Whitney test or a Student-Newman-Keuls *a posteriori* range test was performed. All data were analysed using the statistical software package SPSS for Windows (SPSS Inc., Chicago, Illinois, USA) and the level of significance was chosen to be 5 per cent.

Finite element (FE) analysis

To determine the magnitude of the stresses and strains in the alveolar support structures during orthodontic load transfer, a FE model was made of a porcine lower first molar, according to a technique previously described (Cattaneo, 2003). Briefly, a bone sample containing the lower right first molar was harvested from a mandible of a 50 kg pig and subsequently scanned with a table-top μ CT scanner with a voxel dimension of 37 μ m, at an energy level of 70 keV (μ CT-40, Scanco Medical, Bassersdorf, Switzerland). The resulting three-dimensional (3D) reconstruction was used to generate a

FE model to simulate the *in vivo* loading of the PDL bone complex. The model consisted of the tooth, the tissues forming the periodontium, and the surrounding alveolar bone, and contained more than 443 970 tetrahedral elements and 80 127 nodes.

The material properties of bone were chosen with all bone elements with an assigned Young's modulus of 12 200 MPa and a Poisson's ratio of 0.3, representing a homogeneous distribution of bone properties. For the PDL, the material behaviour was assumed to be non-linear: in compression the PDL was described with a Young's modulus of 0.005 MPa up to 93 per cent strain level after which a Young's modulus of 8.5 MPa was used to simulate pre-contact between the roots and the surrounding bone. In tension, Young's modulus gradually increased from 0.044 MPa at 0 strain to 0.44 MPa at about 50 per cent strain, after which a smaller Young's modulus of 0.032 MPa was used to simulate fibre disruption. The initial and final stiffness were adapted from the values found in the literature (Vollmer *et al.*, 1999; Poppe *et al.*, 2002). The elements representing the tooth were assigned a Young's modulus of 22 000 MPa and a Poisson's ratio of 0.3 (Tanne *et al.*, 1987; Bourauel *et al.*, 1999; Verdonschot *et al.*, 2001).

The model was loaded simulating the loading regime from the experiment by applying a force of 130 cN to the buccal surface of the crown acting in a lingual-buccal direction (Figure 1).

Microtomography of the alveolar tissues

To obtain an insight into the 3D structure of the porcine alveolar bone in the vicinity of the PDL, high-resolution μ CT scans were obtained. For this purpose, a sample of a molar with the surrounding bone from a 3-month-old male pig was embedded in methylmethacrylate. From this a $3 \times 3 \times 7$ mm³ block was cut, taking care that it contained a piece of the root, the entire width of the PDL, and a piece of the alveolar bone. This block was then scanned with a synchrotron radiation-based microtomography system at the BW2-beamline of the DORIS-ring at the German Institute for Synchrotron Radiation (DESY, Hamburg, Germany). Scanning was performed at an energy level of 24 keV and with a spatial resolution of 3.8 μ m. Projections were taken from 0 to 180 degrees in steps of 0.25 degrees. The samples were scanned perpendicular to the long axis of the root. Single slice reconstructions were calculated from the raw data (sinograms) using IDL software (Research Systems Inc., Colorado, USA). These images were then subsequently stacked to create a voxel data set which was read into special visualization software (VGStudio, Volume Graphics GmbH, Heidelberg, Germany) to make the 3D reconstruction images (Dalstra *et al.*, 2003).

Results

Animal study

The orthodontic device successfully moved the teeth buccally and this was clinically detectable from day 2 (Figure 2). Three animals (one from the 7-day and two from the 15-day group) lost the appliance during treatment, and thus the total sample size decreased to 22 animals. The mean force decay was 16, 40, 20, 46 and 56 cN in the five groups. On morphological examination, all buccal sides, both loaded and unloaded, appeared more scalloped than the lingual ones. The periodontal fibres had a different orientation on the buccal and lingual sides, being more elongated on the lingual side (Figure 3). On the buccal, treated side, the surface of the lamina dura was even more scalloped than on the contralateral side, giving an overall picture of a surface undergoing remodelling. On the same side, root resorption could be observed. Root resorption also appeared on the lingual aspect of the treated teeth.

Bone microcracks could be detected on the alveolar bone facing the PDL (Figure 4). Another frequently observed morphological characteristic was the presence of diffuse damage, on both the loaded and unloaded teeth and on both sides, although on the lingual side the orientation of this damage clearly mirrored the orientation of the periodontal fibres (Figure 5). However, as the 'length' of this type of damage was shorter than the range used for the definition of cracks in this article, it was not measured. Double measurements revealed a value of 1.0 mm^{-2} as the error of the method for crack density. This value was smaller than the standard deviation in either of the two sets of double measurements (4.2 and 3.6 mm^{-2}), thus confirming the validity of the method.

Statistical analysis of the mean crack density revealed that the buccal treated side had significantly more cracks than the buccal untreated side at day 1 (Table 1). This difference was significantly larger than that observed at days 2, 7 and 15 (Figure 6). The buccal treated side showed significantly more microcracks than the lingual treated side at day 1 (Table 1), and this difference was larger than that observed at day 15.

FE analysis

FE analysis revealed that the displacement of the molar was such that the molar rotated around a parasagittal axis running approximately through the two apices of the mesial and distal root, corresponding to a controlled buccal tipping. In addition to this tipping, some distal rotation occurred. The combination of these two displacement components and the non-linear PDL generated a complex stress/strain distribution in the alveolar bone. Although from the buccal tipping alone, tensile stresses and strains would be expected in the lingual cervical



Figure 2 Orthodontic tooth movement after 15 days of treatment.



Figure 3 A $100 \mu\text{m}$ section under transmitted light microscopy of treated (T) and untreated (U) molars after 15 days of force application. Note the enlarged periodontal space on the buccal (B) compared with the lingual (L) side on the treated molar. The orientation of the periodontal fibres differs on the buccal and lingual sides. Bar = 1 mm.

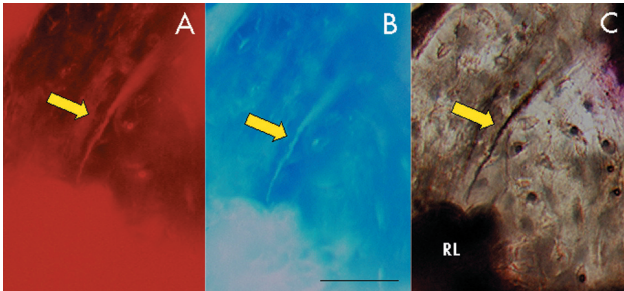


Figure 4 A single microcrack (arrow) in the alveolar bone under green (A) and ultraviolet (B) epifluorescence and transmitted light (C) close to a resorption lacuna (RL) on the buccal treated side at day 1. Bar = 50 μ m.

region of the alveolar bone, the distal rotation also caused tensile stresses and strains in the distal half of the buccal cervical region. Looking at the equivalent strain (strain density), the highest strains occurred in the cervical region (~ 50 μ strain); in the apical region the strains were well below 10 μ strain (Figure 7).

Microtomography of the alveolar support structures

The high-resolution μ CT scan and the following 3D reconstruction enabled a thorough description of the structure of the alveolar bone close to the PDL. As shown in Figure 8, what is defined as the 'lamina dura' is characterized by an extremely irregular surface penetrated by the periodontal fibres. The high scanning resolution allowed identification of the close relationship between the fibres, blood vessels and osteocyte lacunae. The removal of the hard tissue in the three-dimensional reconstruction shows the intricate network of the periodontal fibres into the alveolar bone and how the latter, as a consequence, has an almost trabecular-like appearance (Figure 8d, e).

Discussion

The present research demonstrates the presence of microcracks and microdamage in porcine alveolar bone. This is consistent with the observation that microdamage is increased due to fatigue cyclic loading

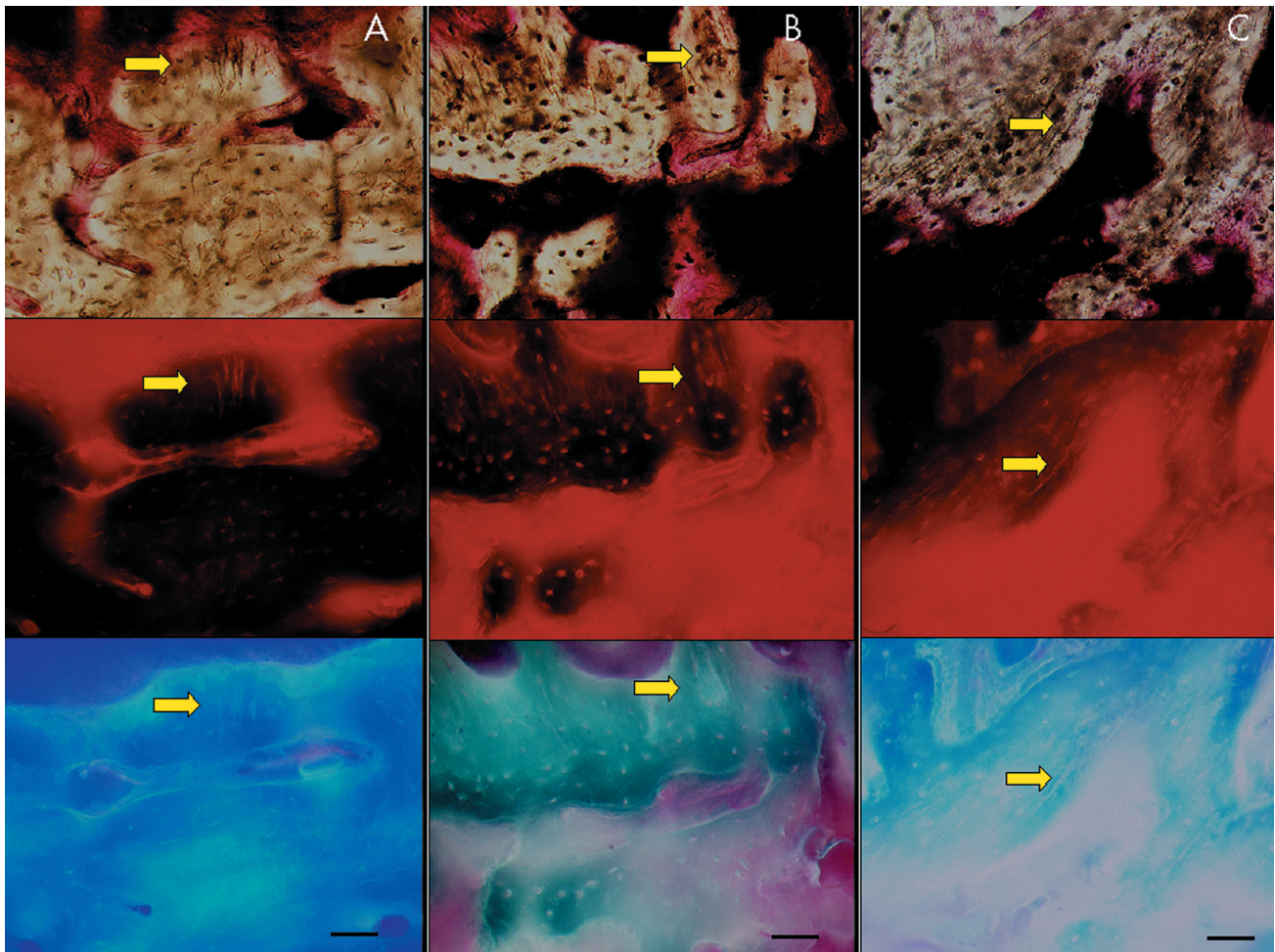


Figure 5 Diffuse microdamage (arrow) in alveolar bone under transmitted light (top), green (middle) and ultraviolet epifluorescence (bottom). (A) Buccal untreated side at day 1, (B) Lingual untreated side at day 2, (C) Buccal treated side at day 2. Bar = 50 μ m.

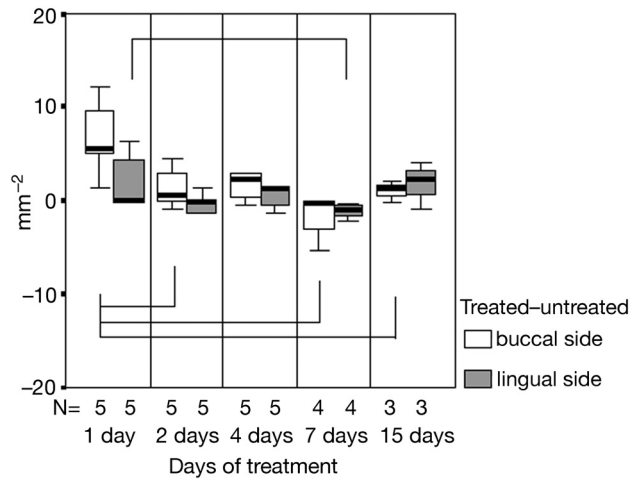


Figure 6 A box plot showing the differences between the treated and untreated sides in crack density (mm^{-2}) on the buccal (white) and lingual (grey) sides. The differences on the buccal side at day 1 were significantly larger than at days 7 and 15, whereas on the lingual side they were significantly different only between days 1 and 7. Bars indicate the statistically significant differences ($P < 0.05$).

(Burr *et al.*, 1985), as mastication or bite function are considered cyclic activities that take place throughout daily activities (Gerstner and Cianfarani, 1998; Miyamoto *et al.*, 1999). Herring *et al.* (2001) found that during mastication, muscle contraction in pigs induces bone strain in the mandible through bite forces. Hence, the presence of microdamage in the mandibular

alveolar bone of pigs may represent the mechanism by which bone adapts to an altered mechanical environment. The PDL acts as the force transducer from the teeth to the alveolar bone. The presence of soft tissue between teeth and bone makes this model different from orthopaedic models, precluding a comparison with published data (Burr *et al.*, 1985; Lee *et al.*, 2000, 2002).

The presence of the PDL made the staining process particularly difficult, as it gave rise to a non-uniform tissue surface. The microanatomy of porcine alveolar bone does not allow for a clear-cut classification into trabecular or cortical bone. As shown in Figure 8, the lamina dura is not dense as usually expected, as it is interrupted by insertion of the periodontal fibres and blood vessels (Figure 8e), both on the buccal and lingual aspects, which gives the bone surface a trabecular appearance. The alveolar wall thus appears porous, with small spiculae facing the PDL (Figure 8c). Those trabeculae mirror the orientation of the periodontal fibres, especially on the lingual aspect (Figure 8). Within the $100\ \mu\text{m}$ thick sections, insertion of the periodontal fibres produces an overlapping of bone tissue and soft tissue, making a new definition of bone microdamage necessary.

As shown in Table 1, the application of a statically determined orthodontic load resulted in an increase and a change in the distribution of cracks. The force applied with the titanium-molybdenum alloy spring made the delivery of the force relatively constant throughout the experimental period, with a decay of only one-third of the initial force level at day 15. The alloy chosen allowed for the use of a thick wire that could resist the chewing

Table 1 Median and quartile crack density (mm^{-2}) in the five groups in the treated and untreated teeth.

Days of treatment		Treated		Untreated	
		Buccal	Lingual	Buccal	Lingual
1 ($n = 5$)	Median	7.7*	0.0	1.6	0.0
	Lower quartile	3.9	0.0	0.5	0.0
	Upper quartile	13.5	6.6	3.2	1.3
2 ($n = 5$)	Median	1.3	1.0	0.9	1.2
	Lower quartile	0.0	0.00	0.35	0.0
	Upper quartile	6.3	1.2	2.8	5.9
4 ($n = 5$)	Median	2.2	1.2	0.6	1.1
	Lower quartile	0.6	0.2	0.2	0.3
	Upper quartile	6.1	5.4	1.4	1.7
7 ($n = 4$)	Median	1.5	0.0	3.7	1.3
	Lower quartile	0.0	0.0	0.5	0.5
	Upper quartile	4.2	0.4	5.6	2.2
15 ($n = 3$)	Median	1.6	3.4	0.0	1.1
	Lower quartile	1.2	1.0	0.0	0.4
	Upper quartile	2.0	4.4	1.8	2.1

*Significantly different from the lingual treated side and from the buccal and lingual untreated sides ($P < 0.05$) at day 1.

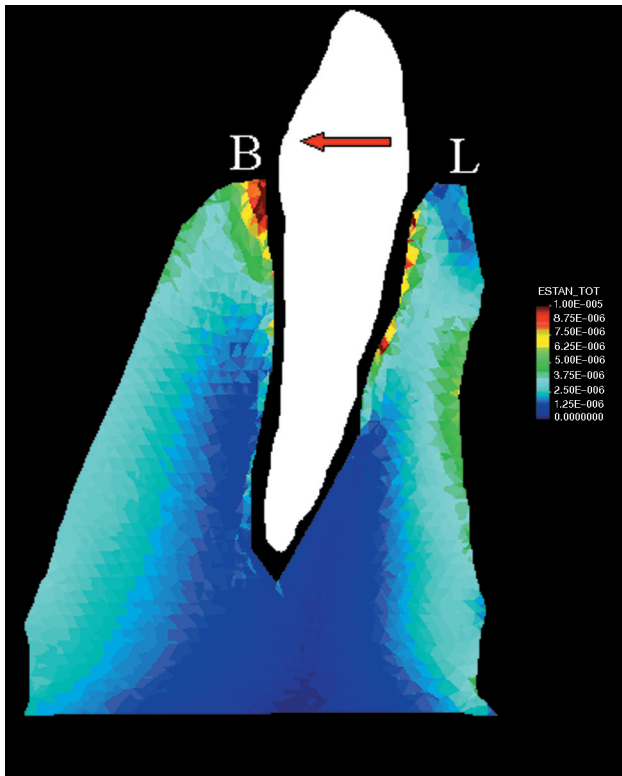


Figure 7 Finite element model demonstrating the distribution of the strains in the alveolar bone on the treated side. Note the higher strain values on the buccal side compared with the lingual side.

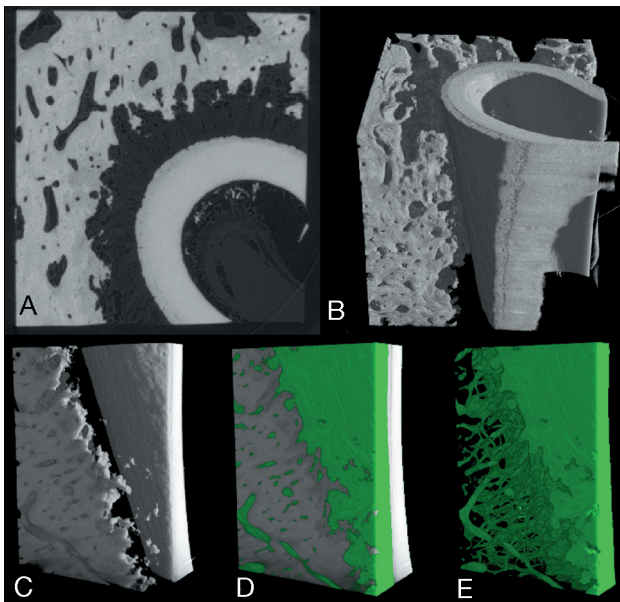


Figure 8 A high-resolution μ CT scan of the mesial root of the first lower molar of a pig. Note the trabecular-like surface of the lamina dura (A, B, C). The subtraction of hard tissue reveals the fine network of soft tissue penetrating the alveolar bone (D, E).

force of the animals. The failure of the appliance in three animals was thus not due to fracture of the cantilever, but to the poor retention of the bands due to the morphology of the porcine molars. The force delivered could be considered intermittent, as the constant force of the cantilever is modulated by the intermittent force delivered by the bite function, acting on both the treated and untreated alveolar processes, as pigs have bilateral occlusion and muscle contraction during mastication (Herring *et al.*, 2001). A possible variation in bite force between animals would not influence the results of this study, as a split-mouth design was used and the paired data analysed. The use of paired data analysis further enabled a statistical evaluation of the data with a small number of animals per group.

The observation of more scalloped surfaces on the buccal than on the lingual side on both the loaded and unloaded teeth could be explained by modelling of the pig's mandible due to growth.

The presence of more cracks buccally on the treated side than on the untreated side might indicate that the orthodontic load induced the formation of more microdamage than that produced by physiological loading alone. Although the presence of bone resorption was not quantified, microcracks (but not diffuse damage) were observed in connection with scalloped surfaces (Figure 4). This is consistent with previous observations of the activation of remodelling in the proximity of microdamage (Burr *et al.*, 1985) and with the targeted activation of remodelling (Lee *et al.*, 2002; Burr, 2002).

Diffuse damage, both on the treated and untreated sides, was also observed (Figure 5). Some authors have related the presence of various types of microdamage to different types of mechanical load, relating tensile strains to diffuse microdamage and compressive strain to linear microcracks (Boyce *et al.*, 1998; Reilly and Currey, 1999). A different distribution pattern of microdamage was also observed according to the mechanical load. In the direction of the force, where the PDL was compressed and the alveolar bone bent, more microcracks than diffuse damage were observed. On the other hand, on the lingual side, where the periodontal fibres were stretched and the alveolar bone was in tension, more diffuse damage was observed.

Quantitative analysis of crack density revealed an extreme variability in crack density distribution of the different sides, sites and treatment groups (Table 1). This could reflect the fact that the presence of the PDL fibres often made the assessment of the sections particularly difficult. However, the error of the method did not reveal any systematic error. The density of microcracks at day 1 was significantly larger on the buccal treated side than on all other sides. The crack density on the treated side then decreased progressively. The latter finding is particularly clear observing the upper quartile values (Table 1). In the following days,

however, paired data analysis did not show any significant difference. This could be explained by the fact that the remodelling process that could remove the cracks had started. Osteoclastic activity usually takes place after the first 2–3 days of force application (Roberts *et al.*, 1981). It has to be underlined that, although cellular activation starts within the first 48 hours after force application in the case of direct resorption, it is improbable that this would be mirrored in a decreased number of cracks, which will need time to disappear. The presence of cracks is a sign of activation of the remodelling cycle, which is assumed to occur over 3 days in humans. At present, no data are available specifically related to the timing of activation of alveolar bone remodelling in pigs loaded by orthodontic forces. Timing varies between species and the availability of cell types associated with the PDL may cause events to be speeded up. It has recently been reported that cracks are removed by becoming filled with calcified matrix, but no time scale is given (Boyde, 2003). As shown in Table 1, the variability in crack density between animals was high. This might contribute to the explanation of the lack of statistically significant results after day 1, as an increased crack density on the untreated buccal side recorded in one animal was observed although no difference in crack density in the buccal untreated side between days was found.

The FE model showed, in the direction of the force, bone strains of a magnitude of approximately 40 μ strain (Figure 7), which is in the range defined by the mechanostat theory of Frost, 'the disuse window', where bone resorption due to disuse starts (Frost, 1994). This is apparently in disagreement with the present results, where more microcracks were found in the direction of the force, the so-called 'compression zone'. However, it should be noted that the FE model used in this study takes only orthodontic loading into consideration. The actual total strains in the alveolar bone will be higher due to functional loading. Furthermore, in the FE model, the alveolar wall was assumed to have a continuous smooth surface. However, as shown in the microtomography 3D reconstruction, the internal wall of the alveolus is a rather rough surface with tiny spiculae extending into the PDL (Figure 8). The bone surfaces that will be exposed to the change in load would thus be the edge of these spiculae and it is likely that the concentration of the load over such small surfaces will lead to the development of microcracks. By including the non-uniform structure of the alveolar wall in a further FE analysis based on high-resolution μ CT scans, this hypothesis could be corroborated.

Conclusions

The localization of microcracks on the side towards which the tooth is moved, where bone resorption is

usually observed, may represent the first damage induced by the orthodontic loading that has to be repaired. Regarding damage repair, it has recently been suggested that bone remodelling induced by microcracks could be an inflammatory repair response (Martin, 2003). The tissue reaction to orthodontic loading is an inflammatory-like response, as orthodontic tooth movement can be modulated by the use of inflammation mediators or anti-inflammatory drugs (Yamasaki *et al.*, 1984; Kehoe *et al.*, 1996). It could therefore be deduced that the mechanical perturbation induced by the orthodontic loading would generate microdamage, thereby producing an inflammatory repair response. Microcracks could thus play a role in the initiation of bone remodelling after orthodontic loading. To corroborate this hypothesis, quantification of resorption sites would be needed. As microcracks have been associated with osteocyte apoptosis (Verborgt *et al.*, 2000; Noble, 2003) and apoptosis has been observed in rats during experimental tooth movement (Hamaya *et al.*, 2002), analysis of the osteocytes in the same areas could be the next step in supporting this preliminary hypothesis.

Address for correspondence

Carlalberta Verna
Department of Orthodontics
Royal Dental College
University of Aarhus
Vennelyst Boulevard 9
8000 Aarhus-C
Denmark

Acknowledgements

This research was sponsored by a W J B Houston Scholarship from the European Orthodontic Society awarded to the first author. We would also like to extend our gratitude to Professor Jens Christian Djurhuus and the staff of the Department for Experimental Clinical Research, Aarhus University, Skejby Hospital, for access to their facilities in the experimental phase of the project. Sussi Madsen, Department of Orthodontics, Royal Dental College, Aarhus, is thanked for her skilled laboratory assistance. The SR-based tomography was supported by IHP contract II-00-64EC of the European Commission.

References

- Bien S M 1966 Hydrodynamic damping of tooth movement. *Journal of Dental Research* 45: 907–914
- Bourauel C, Freudenreich D, Vollmer D, Kobe D, Drescher D, Jäger A 1999 Simulation of orthodontic tooth movements. A comparison of numerical models. *Journal of Orofacial Orthopedics* 60: 136–151

- Boyce T M, Fyhrie D P, Glotkowski M C, Radin E L, Schaffler M B 1998 Damage type and strain mode associations in human compact bone bending fatigue. *Journal of Orthopaedic Research* 16: 322–329
- Boyde A 2003 The real response of bone to exercise. *Journal of Anatomy* 203: 173–189
- Burr D B 2002 Targeted and nontargeted remodeling. *Bone* 30: 2–4
- Burr D B, Martin R B, Schaffler M B, Radin E L 1985 Bone remodeling in response to *in vivo* fatigue microdamage. *Journal of Biomechanics* 18: 189–200
- Cattaneo P M 2003 Orthodontic aspects of bone mechanics and bone remodelling. Thesis, University of Aarhus, Denmark
- Dalstra M, Cattaneo P M, Beckmann F, Hauge E M 2003 Microtomography of cortical bone using a synchrotron source. In: Hamza H M (ed.) *Proceedings of the IASTED International Conference on Biomechanics*. ACTA Press, Anaheim, pp. 283–287
- Davidovitch Z, Finkelson M D, Steigman S, Shanfeld J L, Montgomery P C, Korostoff E 1980 Electric currents, bone remodeling, and orthodontic tooth movement. I. The effect of electric currents on periodontal cyclic nucleotides. *American Journal of Orthodontics* 77: 14–32
- Davidovitch Z, Nicolay O F, Ngan P W, Shanfeld J L 1988 Neurotransmitters, cytokines, and the control of alveolar bone remodeling in orthodontics. *Dental Clinics of North America* 32: 411–435
- Epker B N, Frost H M 1965 Correlation of bone resorption and formation with the physical behavior of loaded bone. *Journal of Dental Research* 44: 33–41
- Frost H M 1960 Presence of microscopic cracks *in vivo* in bone. *Henry Ford Hospital Medical Bulletin* 8: 25–35
- Frost H M 1994 Wolff's Law and bone's structural adaptations to mechanical usage: an overview for clinicians. *Angle Orthodontist* 64: 175–188
- Gerstner G E 1998 Intermittency in mastication and apomorphine-induced gnawing. *Physiology and Behavior* 65: 569–574
- Gerstner G E, Cianfarani T 1998 Temporal dynamics of human masticatory sequences. *Physiology and Behavior* 64: 457–461
- Hamaya M, Mizoguchi I, Sakakura Y, Yajima T, Abiko Y 2002 Cell death of osteocytes occurs in rat alveolar bone during experimental tooth movement. *Calcified Tissue International* 70: 117–126
- Heller I J, Nanda R 1979 Effect of metabolic alteration of periodontal fibers on orthodontic tooth movement. An experimental study. *American Journal of Orthodontics* 75: 239–258
- Herring S W, Rafferty K L, Liu Z J, Marshall C D 2001 Jaw muscles and the skull in mammals: the biomechanics of mastication. *Comparative Biochemistry and Physiology. Part A, Molecular and Integrative Physiology* 131: 207–219
- Houston W J B 1983 The analysis of errors in orthodontic measurements. *American Journal of Orthodontics* 83: 382–390
- Kehoe M J, Cohen S M, Zarrinnia K, Cowan A 1996 The effect of acetaminophen, ibuprofen, and misoprostol on prostaglandin E2 synthesis and the degree and rate of orthodontic tooth movement. *Angle Orthodontist* 66: 339–349
- Lee T C, Myers E R, Hayes W C 1998 Fluorescence-aided detection of microdamage in compact bone. Part 2, *Journal of Anatomy* 193: 179–184
- Lee T C, O'Brien F J, Taylor D 2000 The nature of fatigue damage in bone. *International Journal of Fatigue* 22: 847–853
- Lee T C, Staines A, Taylor D 2002 Bone adaptation to load: microdamage as a stimulus for bone remodelling. *Journal of Anatomy* 201: 437–446
- Marotti G 1996 The structure of bone tissues and the cellular control of their deposition. *Italian Journal of Anatomy and Embryology* 101: 25–79
- Martin R B 2003 Fatigue microdamage as an essential element of bone mechanics and biology. *Calcified Tissue International* 73: 101–107
- Melsen B 2001 Tissue reaction to orthodontic tooth movement—a new paradigm. *European Journal of Orthodontics* 23: 671–681
- Miyamoto K, Ishizuka Y, Ueda H M, Saifuddin M, Shikata N, Tanne K 1999 Masseter muscle activity during the whole day in children and young adults. *Journal of Oral Rehabilitation* 26: 858–864
- Noble B 2003 Bone microdamage and cell apoptosis. *European Cells and Materials* 6: 46–55
- Parfitt A M 2002 Targeted and nontargeted bone remodeling: relationship to basic multicellular unit origination and progression. *Bone* 30: 5–7
- Poppe M, Bourauel C, Jäger A 2002 Determination of the elasticity parameters of the human periodontal ligament and the location of the center of resistance of single-rooted teeth. A study of autopsy specimens and their conversion into finite element models. *Journal of Orofacial Orthopedics* 63: 358–370
- Reilly G C, Currey J D 1999 The development of microcracking and failure in bone depends on the loading mode to which it is adapted. *Journal of Experimental Biology* 202: 543–552
- Reitan K 1967 Clinical and histologic observations on tooth movement during and after orthodontic treatment. *American Journal of Orthodontics* 53: 721–745
- Reitan K, Rygh P 1994 Biomechanical principles and reactions. In: Graber T M, Vanarsdall R L (eds) *Orthodontics: current orthodontic concept and techniques*. C V Mosby, St. Louis, pp. 96–192
- Roberts W E, Goodwin W C J, Heiner S R 1981 Cellular response to orthodontic force. *Dental Clinics of North America* 25: 3–17
- Sandy J R, Farndale R W, Meikle M C 1993 Recent advances in understanding mechanically induced bone remodeling and their relevance to orthodontic theory and practice. *American Journal of Orthodontics and Dentofacial Orthopedics* 103: 212–222
- Tanne K, Sakuda M, Burstone C J 1987 Three-dimensional finite-element analysis for stress in the periodontal tissue by orthodontic forces. *American Journal of Orthodontics and Dentofacial Orthopedics* 92: 499–505
- Tuncay O C, Ho D, Barker M K 1994 Oxygen tension regulates osteoblast function. *American Journal of Orthodontics and Dentofacial Orthopedics* 105: 457–463
- Verborgt O, Gibson G J, Schaffler M B 2000 Loss of osteocyte integrity in association with microdamage and bone remodeling after fatigue *in vivo*. *Journal of Bone and Mineral Research* 15: 60–67
- Verdonschot N, Fennis W M, Kuijs R H, Stolk J, Kreulen C M, Creugers N H 2001 Generation of 3-D finite element models of restored human teeth using micro-CT techniques. *International Journal of Prosthodontics* 14: 310–315
- Vollmer D, Bourauel C, Maier K, Jäger A 1999 Determination of the centre of resistance in an upper human canine and idealized tooth model. *European Journal of Orthodontics* 21: 633–648
- Weinbaum S, Cowin S C, Zeng Y 1994 A model for the excitation of osteocytes by mechanical loading-induced bone fluid shear stresses. *Journal of Biomechanics* 27: 339–360
- Yamasaki K, Shibata Y, Imai S, Tani Y, Shibasaki Y, Fukuhara T 1984 Clinical application of prostaglandin E1 (PGE1) upon orthodontic tooth movement. *American Journal of Orthodontics* 85: 508–518
- Zengo A N, Pawluk R J, Bassett C A 1973 Stress-induced bioelectric potentials in the dentoalveolar complex. *American Journal of Orthodontics* 64: 17–27

Copyright of European Journal of Orthodontics is the property of Oxford University Press / UK and its content may not be copied or emailed to multiple sites or posted to a listserv without the copyright holder's express written permission. However, users may print, download, or email articles for individual use.